Crystal Structure of the Malic Enzyme from *Ascaris suum* Complexed with Nicotinamide Adenine Dinucleotide at 2.3 Å Resolution[†,‡]

David E. Coleman,[§] G. S. Jagannatha Rao,[||] E. J. Goldsmith,[§] Paul F. Cook,[⊥] and Ben G. Harris*[,||]

Department of Molecular Biology and Immunology, University of North Texas Health Science Center, Fort Worth, Texas 76107, Department of Biochemistry, The University of Texas Southwestern Medical Center, 5323 Harry Hines Boulevard, Dallas, Texas 75235-9050, and Department of Chemistry and Biochemistry, University of Oklahoma, Norman, Oklahoma 73019

Received January 7, 2002; Revised Manuscript Received March 28, 2002

ABSTRACT: The structure of the *Ascaris suum* mitochondrial NAD−malic enzyme in binary complex with NAD has been solved to a resolution of 2.3 Å by X-ray crystallography. The structure resembles that of the human mitochondrial enzyme determined in complex with NAD [Xu, Y., Bhargava, G., Wu, H., Loeber, G., and Tong, L. (1999) *Structure 7*, 877−889]. The enzyme is a tetramer comprised of subunits possessing four domains organized in an "open" structure typical of the NAD-bound form. The subunit organization, as in the human enzyme, is a dimer of dimers. The *Ascaris* enzyme contains 30 additional residues at its amino terminus relative to the human enzyme. These residues significantly increase the interactions that promote tetramer formation and give rise to different subunit−subunit interactions. Unlike the mammalian enzyme, the *Ascaris* malic enzyme is not regulated by ATP, and no ATP binding site is observed in this structure. Although the active sites of the two enzymes are similar, residues interacting with NAD differ between the two. The structure is discussed in terms of the mechanism and particularly with respect to previously obtained kinetic and site-directed mutagenesis experiments.

Malic enzymes (MEs)[1] catalyze the oxidative decarboxylation of L-malate to pyruvate and carbon dioxide, using divalent metal ions (e.g., Mg^{2+} or Mn^{2+}) and NAD or NADP as cofactors (Scheme 1). Malic enzymes have been found in representatives of all of the major biological divisions and participate in diverse metabolic pathways such as photosynthesis, lipogenesis, and energy metabolism of parasitic helminths (*3*−*9*). In eukaryotes, cytoplasmic, mitochondrial, and chloroplastic isoforms have been identified (*10*−*12*). Metazoan isoforms include cytosolic NADP-dependent ME (c-NADP-ME), mitochondrial NADP-dependent ME, and mitochondrial NAD-dependent ME (m-NAD-ME) (e.g., ref *13*). Mitochondrial NAD-MEs may use either NAD or NADP in vitro (and thus may be referred to as having "dual specificity") but most likely use NAD in vivo (*14*) because of their location within mitochondria.

Scheme 1

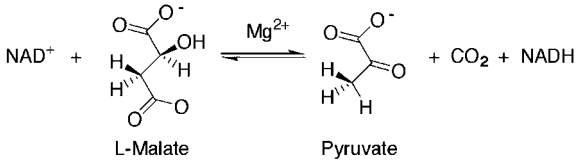

Malic enzymes generally form homotetramers with monomer molecular masses in the range 60−80 kDa (*15*). A sequence comparison of MEs indicates significant homology within the family. In contrast, with the exception of two dinucleotide binding signature motifs, the members of this family have no observed overall homology to other proteins (*15*). Structural studies of human ME indicate that these enzymes belong to a new class of oxidative decarboxylases (*16*).

Several crystal structures of human mitochondrial NAD-ME in complex with various ligands have been reported (*17*). These structures include a binary complex with NAD alone (*16*, *18*), a ternary complex with NAD and Lu^{2+} (an inhibitor of the enzyme) (*19*), and quaternary complexes with NAD, Mg^{2+}, and tartronate (a dead-end analogue of L-malate) or NAD, Mn^{2+}, and oxalate (a dead-end analogue of enolpyruvate) or NAD, Mg^{2+}, and ketomalonate (a dead-end analogue of oxalacetate/pyruvate) (*20*). This ensemble of structures defined two major conformational forms. The active site in the binary complex is in an "open" form, ready to accept the metal ion and L-malate, while the active sites of the quaternary complexes are in a "closed" form, presumably

[†]This work was supported by grants to B.G.H. from the National Institutes of Health (AI24155, AI41552) and the Robert A. Welch Foundation (BK1309), to P.F.C. from the Oklahoma Center for Advancement of Science and Technology (HR 990217), the American Chemical Society (PRF 35894-AC4), and the National Science Foundation (MCB 0091207), and to E.J.G. from the Welch Foundation (I1128).

[‡] The coordinates have been deposited in the RCSB Protein Databank, Accession Number 1LLQ.

* To whom correspondence to should be addressed. E-mail: bharris@hsc.unt.edu. Phone: 817-735-2126. Fax: 817-735-2133.

[§] The University of Texas Southwestern Medical Center.

[||] University of North Texas Health Science Center.

[⊥] University of Oklahoma.

[1] Abbreviations: NAD, nicotinamide adenine dinucleotide; NADH, reduced nicotinamide adenine dinucleotide; NADP, nicotinamide adenine dinucleotide phosphate; NADPH, reduced nicotinamide adenine dinucleotide phosphate; ME, malic enzyme; c-NADP-ME, cytosolic NADP-dependent ME; m-NADP-ME, mitochondrial NADP-dependent malic enzyme; m-NAD-ME, mitochondrial dual specificity (NAD or NADP) dependent malic enzyme; DTT, dithiothreitol; EDTA, ethylenediaminetetraacetic acid.

10.1021/bi0255120 CCC: $22.00
Published on Web 05/09/2002

primed to catalyze the reaction. The location and mode of binding of reactants are suggested by the closed form structures. In all of these structures the homotetramer contains two unique interfaces (e.g., Figure 8): an extensive interface between two monomers (the dimer interface) and a less extensive interface between the two dimers (the tetramer interface). The quaternary structure of the tetramer is thus a dimer of dimers. The different complexes exhibit differences between their quaternary structures, implying that ligand binding may be linked to changes in the quaternary state. In all of these human m-NAD-ME structures, electron density corresponding to the adenosine moiety of a second NAD molecule was observed at each of four sites located between subunits within the tetramer interface referred to as "exo NAD sites". Human m-NAD-ME is allosterically inhibited by ATP (*13*), and thus the exo NAD sites likely represent the ATP inhibitory sites (*16*). Because the inhibitory site is filled in all of these human m-NAD-ME structures, it is not clear whether any of the structures represent an active form. The binary and quaternary complexes also exhibit different tetrameric organizations.

The mitochondrial NAD-dependent malic enzyme (m-NAD-ME) from the parasitic roundworm *Ascaris suum* is the object of this structural study. *Ascaris* m-NAD-ME is involved in the production of energy from glucose and other food sources and thus serves an important role in the basic metabolism of the organism (*2*, *9*, *21*). As the NADH generated in the reaction catalyzed by this enzyme is the sole source of reducing equivalents, the enzyme is a potential chemotherapeutic target against ascariasis. The sequence homology between human and *Ascaris* m-NAD-MEs is 82% (Figure 1),[2] and thus one would expect the three-dimensional structures for the two enzymes to be similar. Functionally, *Ascaris* m-NAD-ME differs from the human enzyme in that it is not allosterically inhibited by ATP. Furthermore, its sequence contains 30 additional residues at its amino terminus in addition to several smaller insertions and deletions (Figure 1). Thus, although the two enzymes are similar, differences between their structures would be expected.

We report here the 2.3 Å crystal structure of m-NAD-ME from *A. suum* in binary complex with NAD.[3] The subunit structure resembles most closely that of the human ME binary complex, suggestive that this open conformation is conserved in evolution. In contrast, the subunit interactions are less well conserved and are influenced by the N-terminal 30-residue extension in the *Ascaris* enzyme and the absence of the ATP regulatory site present in the mammalian protein.

MATERIALS AND METHODS

Purification of Malic Enzyme. Malic enzyme was purified by slight modifications of the procedure described in Clancy et al. (*22*). Briefly, homogenates of *A. suum* were subjected to ammonium sulfate fractionation and ion-exchange chromatography on DEAE-Sephacyl and phosphocellulose (*22*). The eluate from phosphocellulose was precipitated by dialysis against saturated ammonium sulfate, and the precipitate was dissolved in 15 mM triethanolamine hydrochloride buffer, pH 7.5, containing 10 mM 2-mercaptoethanol and 5% glycerol (v/v) and dialyzed overnight against 4 L of the same buffer. The dialysate was subjected to affinity chromatography on blue and orange Sepharose as described by Karsten and Cook (*23*). The eluate from orange Sepharose was concentrated by dialysis against saturated ammonium sulfate and the precipitate dissolved in 4−5 mL of storage buffer containing 15 mM triethanolamine−maleate, pH 7.5, 5 mM DTT, and 10% glycerol (v/v). Samples were stored at −20 °C.

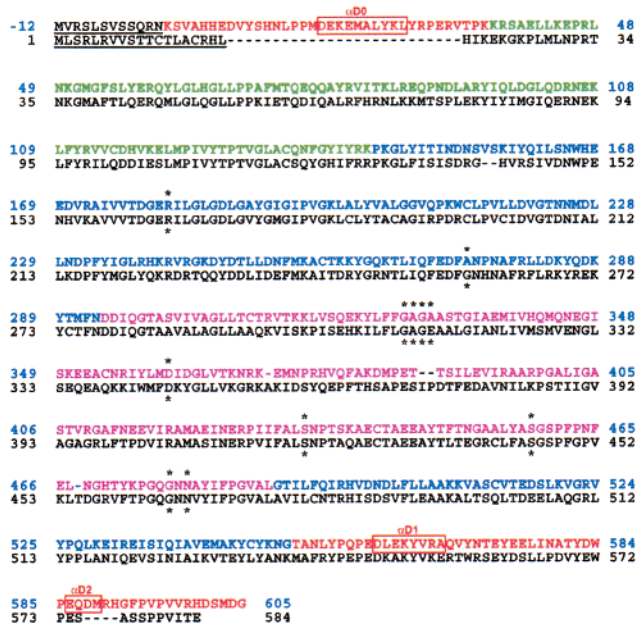

FIGURE 1: Sequence alignment of the *Ascaris* (upper rows) and human (lower rows) m-NAD-ME. The *Ascaris* residues are colored by domain: green, A domain; blue, B domain; magenta, C domain; red, D domain. Secondary structural elements for the D domain are indicated. Underlined residues contain a mitochondrial translocation signal sequence and were not present in the m-NAD-ME used for both the *Ascaris* and human structural studies. Residues involved in NAD binding are indicated by stars.

Crystallization and X-ray Data Collection. The crystals used for data collection were obtained by the hanging drop−vapor diffusion method described earlier [Clancy et al. (*22*)]. However, the concentrations of the additives were different (5 mM NAD, 10 mM tartronate, and 20 mM $MgSO_4$ instead of 7 mM NAD, 87 mM tartronate, and 87 mM $MgSO_4$ used previously). The crystals belong to space group $P3_121$ with a and b = 130.62 Å and c = 149.23 Å and contain two molecules per asymmetric unit (*22*). For cryoprotection, crystals were first soaked overnight in a solution containing 25% (w/v) PEG 4000, 15 mM NAD, and 10 mM 2-mercaptoethanol in 100 mM Tris−SO_4, pH 7.5, and then sequentially transferred into the above solution containing 5%, 10%, 15%, and finally 20% ethylene glycol (v/v). Crystals were allowed to soak in each solution for approximately 20 min and were left overnight in the final solution. Crystals were flash frozen in liquid propane and stored in liquid nitrogen prior to data collection. X-ray diffraction data to 2.3 Å were collected at the Cornell synchrotron source (CHESS) F1 line (λ = 0.947 Å) equipped with a CCD detector (Table 1). Data were processed using the DENZO/SCALEPACK programming package (*24*). Data collection statistics are given in Table 1.

[2] The residue -numbering scheme of *Ascaris* m-NAD-ME corresponds to N-12 of those reported in Kulkarni et al. (*1*).

[3] A brief description of this molecule has been previously reported in ref *2*.

Table 1: Data Collection and Refinement Statistics

total observations	308683
unique observations	62146
resolution (Å)	25.0−2.3
completeness	94.6
R_{merge}[a]	4.7
$\langle I/\sigma \rangle$	30
R[b]	24.7 (25−2.3 Å)
R_{free}[c]	28.0 (25−2.3 Å)
protein atoms	9045
solvent atoms	74

[a] $R_{merge} = 100(\sum_h \sum_i |I_{hi} - \langle I_h \rangle| / \sum_h \sum_i |I_{hi}|)$. [b] $R = 100(\sum_h |F_{ho} - F_{hc}| / \sum_h |F_{ho}|)$. [c] $R_{free} = R$ for a randomly selected 5% of the data excluded from the refinement.

Model Building and Refinement. The structure was determined using the molecular replacement method (*25*). The AMORE module of the CCP4 package (*26*) was used to determine the orientation of the two crystallographically independent subunits (α_a and α_b) using a single monomer from the human m-NAD-ME·NAD binary complex [PDB accession code 1QR6 (*16*)] as the search model. The orientation of the two crystallographically independent monomers formed a dimer in the asymmetric unit related by 2-fold noncrystallographic symmetry. Packing of this dimer within the unit cell generated a tetrameric complex ($\alpha_a\alpha_b\alpha_c\alpha_d$) having 222 symmetry as observed in the human enzyme (the noncrystallographic 2-fold axis lies in the plane corresponding to the dimer interface whereas a crystallographic 2-fold axis lies in the plane corresponding to the tetramer interface; see Figure 5). However, the quaternary structure of the tetramer was somewhat different than that observed in the human enzyme.

The initial model underwent simulated annealing refinement with strict NCS constraints using the CNS (v0.9) programming package (*27*). Initial σA-weighted $2F_o - F_c$ and $F_o - F_c$ maps (*28*) indicated differences between the *Ascaris* and human enzymes, particularly in the amino- and carboxyl-terminal regions. The model was manually rebuilt using the interactive graphics model building program O (*29*). Differences between the two crystallographically independent subunits were observed, and independent models were used for each monomer after the first two rounds of refinement. NCS-restrained positional and grouped temperature factor refinement was carried out on the rebuilt model using CNS followed by additional rounds of model building and refinement. The NCS restraints were reduced during subsequent rounds of refinement, and a full atomic temperature factor refinement was carried out. A bulk solvent correction (*30*) was applied throughout all refinements, and the free R factor method was used to monitor the refinement (*31*). Density for the NAD cofactor was present in the active site, and NAD was added during the first round of model building. No evidence of additional NAD binding sites corresponding to the exo NAD sites in human ME was observed. Although both tartronate and Mg^{2+} were included in the crystallization solutions, no indications of their presence within the active site were observed. Carboxyl-terminal residues 594−600 of one crystallographically independent monomer (α_a) are represented by good density and were unambiguously modeled whereas there is no interpretable density for the corresponding residues of the second monomer (α_b). The carboxyl-terminal residues of the α_a subunit are packed against the adjacent monomer of a crystallographically related tetramer, and this likely explains their higher degree of order. The current model contains residues 2−600[2] (α_a) and residues 2−593 (α_b) of the two crystallographically independent subunits, 2 NAD molecules bound in the active sites, and 74 water molecules. The two crystallographically independent subunits superimpose with a root mean square (rms) difference of 0.12 Å between 592 corresponding α carbons. The structure exhibits good stereochemistry, with 89% of the residues in the most favored region of the Ramachandran plot as analyzed by PROCHECK (*32*). Final refinement statistics calculated using all data are given in Table 1. Comparisons between subunits and domains and with the human ME structures were carried out using O. Buried surfaces were calculated using CNS.

RESULTS

Structure of the Monomer. With the exception of the additional residues at the amino and carboxyl termini, the architecture and topology of the *Ascaris* m-NAD-ME monomer are similar to those of the human enzyme. Briefly, the monomer (Figure 2) is composed of four domains (A−D), which correspond to those assigned by Xu et al. for the human enzyme (*16*). Domain A (residues 37−144) is α-helical and domain B (residues 145−293 and 479−550) is an α/β-type domain. Both domains are involved in the dimer and tetramer interactions, and the A and B domains together may be considered to constitute the core of the molecule. Domain C (residues 294−478) is an insert into the B domain and contains a Rossmann dinucleotide binding domain (*33*) to which the NAD cofactor is bound. As per human ME, the dinucleotide binding domain differs from a canonical Rossmann fold in that there is no β strand corresponding to the third β strand of a Rossmann fold. The region that would be occupied by this strand is filled by a β hairpin turn and an antiparallel β strand (361−366), followed by a segment (367−389) that contains a short helix (375−380). Domain C is the most poorly ordered domain, as indicated by weak electron density and its higher overall temperature factor ($\langle B_C \rangle = 70.0$ Å^2) relative to those of the other domains ($\langle B_A \rangle = 42.8$ Å^2, $\langle B_B \rangle = 45.5$ Å^2, $\langle B_D \rangle = 50.8$ Å^2).

Domain D (Figure 2) is composed of the amino-terminal (2−36) and carboxyl-terminal (551−600) residues and contains structural features unique to *Ascaris* ME (Figures 1 and 2). Most of the carboxyl-terminal segment is similar to that of human ME and consists of a segment of random coil followed by a helix (αD1, 561−568) followed by an extended β strand-like coil (569−585) which is packed against the amino-terminal portion of the D domain. The remaining carboxyl-terminal residues are not present in human ME and form a short four-residue helix (αD2, residues 586−589) and a random coil (residues 590−600). The amino-terminal segment of domain D (residues 2−36) contains residues (2−32) that are not found in human ME (Figure 1). This segment of the D domain begins as a coil (residues 2−5) which packs against D domain carboxyl-terminal residues 582−584. This is followed by a coil (6−18) that leads to helix αD0 (19−28) and a coil (29−36) which links it to domain A. There are numerous intradomain interactions within domain D (e.g., between αD0 and αD1),

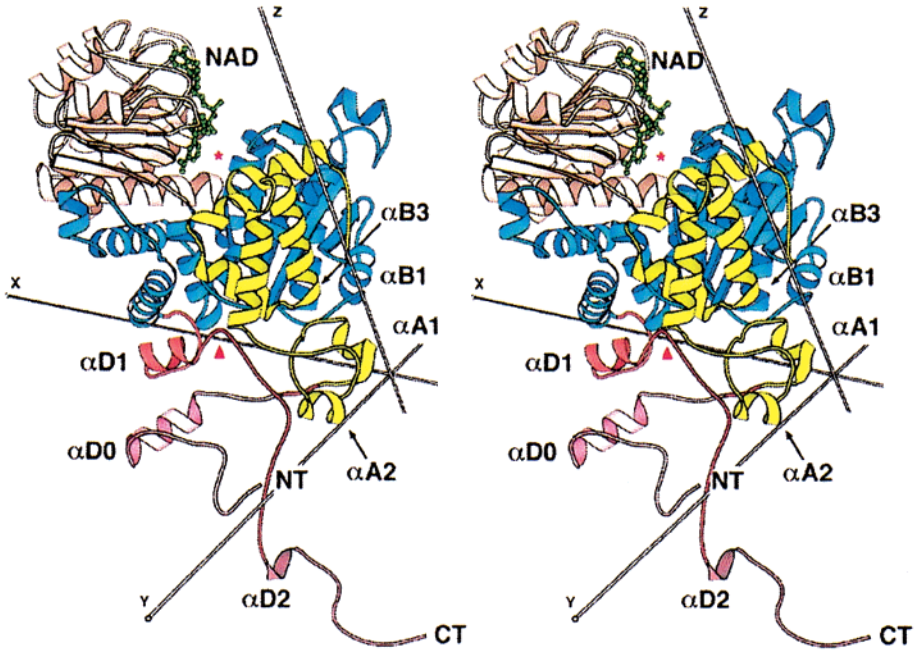

FIGURE 2: Structure of the monomer of m-NAD-ME from *A. suum* in binary complex with NAD. The NAD ligand and the amino and carboxyl termini are indicated, and the four domains are colored as follows: yellow, A domain; blue, B domain; tan, C domain; red and purple, D domain. The secondary structures discussed in the text are also labeled. The purple segment of D domain contains the amino terminus and helix αD0 and corresponds to residues that are not present in human ME. The region that corresponds to the metal and substrate binding site in the human ME quaternary complexes is indicated by a red star, and the region that corresponds to the exo NAD site in human ME is indicated by a red triangle. The axes labeled *X*, *Y*, and *Z* correspond to the 2-fold rotation axes of the tetramer; axis *X* corresponds to the crystallographic 2-fold. [This figure and Figures 3−5 and 7 were generated using the program MOLSCRIPT (*49*).]

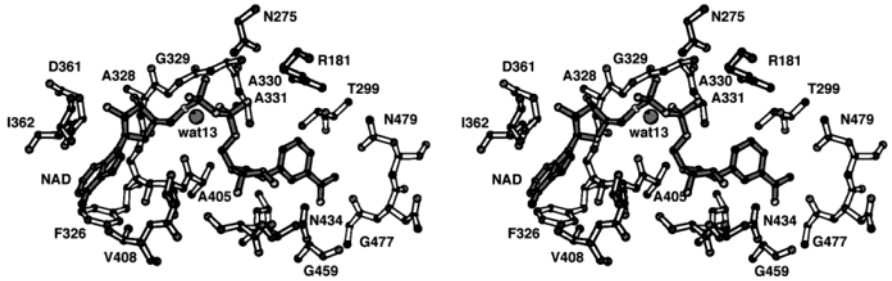

FIGURE 3: NAD binding site in the *Ascaris* ME·NAD complex. NAD, a water molecule (wat13), and key residues are labeled.

but many interactions are made with other subunits within the tetramer as discussed below.

The Active Site. The active site has been identified by the location of the NAD cofactor (Figure 2) and by comparison with the closed and open form of human ME. Comparison with human ME complexes indicates that the active site in the *Ascaris* ME binary complex is most similar to the open ME·NAD binary complex of the human enzyme. The active site residues are contributed primarily by domains B and C, with one residue (Y126) being contributed by domain A.

The NAD cofactor is bound in the anti conformation, with the *re* face of the nicotinamide moiety exposed to the solvent, and interacts only with residues of the C domain (Figure 3). The adenosine moiety of the NAD cofactor is bound by three loops (361−362, 326−329, and 405−408) in which the side chains of residues I362, F326, and V408 form a hydrophobic pocket for adenine. Key residues within the NAD binding site for the *Ascaris* binary complex are indicated in Figure 3 and are listed in Table 2 along with interaction distances. For comparison, the homologous residues and distances in the human ME binary complex are also given in Table 2. Many of the NAD−enzyme interactions in the *Ascaris* and human binary complexes are identical, but the binding mode of NAD differs between the two enzymes in several ways. As indicated by the interaction distances in Table 2, two NAD−residue interactions that are present in the human binary complex are absent in *Ascaris*. In the human binary complex, the Nω amino group of R165 makes a salt bridge with the NO1 oxygen of NAD (3.0 Å) and is the sole interaction between NAD and the B domain. In *Ascaris*, the nearest atom of the homologous residue (R181) is 4.1 Å away and thus does not contribute to NAD binding; instead, the guanidinium group of R181 forms a salt bridge with the carboxyl moieties of E272 and D295 (Figure 4). The Nδ amino group of N259 in the human binary complex forms a hydrogen bond with the AO1 oxygen of NAD (2.7 Å), but the corresponding distance (3.8 Å) for the homologous *Ascaris* residue (N275) indicates no interaction. In *Ascaris*, a water molecule (wat13) is hydrogen bonded to the NO2 oxygen of NAD and may compensate, in part, for the loss of interactions with R181 and N259.

Several residues in *Ascaris* ME have been directly implicated in metal−substrate binding and substrate catalysis on the basis of physical, chemical, and mutagenic studies

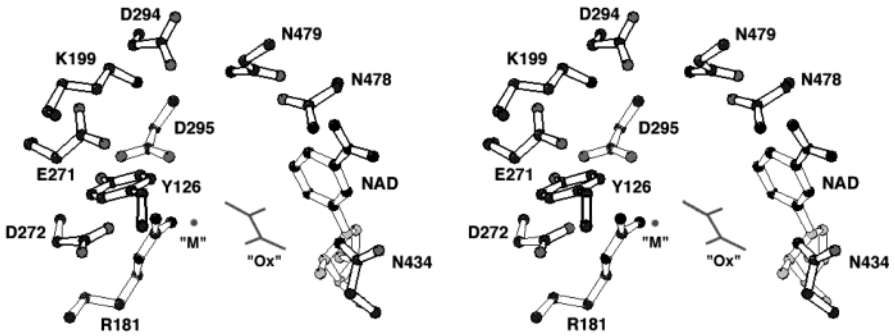

FIGURE 4: Active site in the *Ascaris* ME·NAD complex showing the nicotinamide moiety of NAD and key residues. For reference, the positions of the Mn^{2+} ion ("M") and oxalate ("Ox") from the human ME·NAD·Mn^{2+}·oxalate complex (positioned by superposition of the corresponding C domains from *Ascaris* and human ME) are shown; these ligands are not present in the *Ascaris* ME binary complex.

Table 2: Interactions between the NAD Cofactor and Residues within the *Ascaris* and Human ME·NAD Binary Complexes[a]

NAD moiety	atoms (NAD/protein)	residues		distance (Å)	
		Ascaris	human	*Ascaris*	human
adenine	AO2′/NH	L362	K346	3.2	3.1
ribose	AO3′/NH	A328	A312	3.1	3.2
	AO3′/NH	G329	G313	3.0	3.4
bisphosphate	NO1/Nω	R181	R165	4.1	3.0
	AO1/Nδ	N275	N259	3.8	2.7
	AO1/NH	A330	E314	2.9	3.3
	NO2/NH	A331	A315	2.9	2.9
	NO2/O	wat13		2.8	
nicotinamide	NO3′/NH	N434	N421	3.1	3.4
ribose	NO2′/NH	N434	N421	3.3	2.8
	NO2′/Nδ	N434	N421	3.2	2.8
nicotinamide	NO7/C	G459	G446	3.3	3.1
	NN7/O	G477	G465	2.7	2.6
	NN7/Oδ	N479	N467	3.0	3.1

[a] A key to the atom names for NAD is as follows:

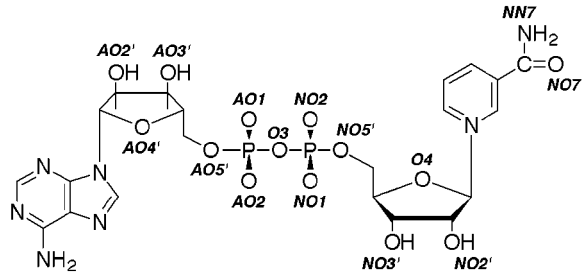

(*2*, *34*−*36*) and by comparison with structures of human ME. Modeling of the position of the metal ion based on the human m-NAD-ME·oxalate·Mn quaternary complex (*20*) indicates that residues implicated in metal binding (E271, D272, D295) are not positioned for metal binding (Figure 4). Likewise, modeling of the position of the transition state analogue oxalate from the human ME quaternary complex in the *Ascaris* ME binary complex indicates that residues implicated in substrate binding and catalysis (R181, K199, D295, N434, and N479) are also poorly positioned for their prospective roles. Thus, in the *Ascaris* ME binary complex, residues involved in NAD binding appear to be positioned effectively for their roles, but otherwise significant rearrangements would be required in order to array active site residues for binding and catalysis.

Structure of the Tetramer. The tetramer exhibits 222 (or D_2) symmetry and is relatively flat (Figures 5 and 8). The α_a and α_b subunits (and likewise α_c and α_d) are related by noncrystallographic 2-fold symmetry whereas the α_a and α_d subunits (and likewise α_b and α_c) are related by crystallographic 2-fold symmetry. A surface area of ~4900 Å^2 per monomer is buried by formation of the tetramer.[4] Formation of the dimer alone results in burial of 1900 Å^2/monomer (which is similar to that observed for human ME), involves residues from the respective A and B domains, and exhibits interactions that are similar to those observed in human ME. Formation of the full tetramer from two dimers then buries an additional 3000 Å^2/monomer. The bulk of this buried surface (2650 Å^2/monomer) involves the amino-terminal (*2*−*36*) and carboxyl-terminal (578−593) residues of the D domain. These residues bridge across the tetramer interface and form interactions with another dimer (Figure 5B). The interactions between carboxyl-terminal residues 578−585 of the α_a subunit with the α_c and α_d subunits bury 1050 Å^2/monomer and are similar to the homologous interactions in human ME. The amino- and carboxyl-terminal segments of *Ascaris* ME provide new tetramer interactions that are not present in human ME. Carboxyl-terminal residues 586−593 of the α_a subunit lie in a crevice formed by residues 53−57, 72−75, and the αA3 helix of the α_c subunit and residues 232−237 of the α_d subunit (Figure 5B). These interactions bury 750 Å^2/monomer of surface area. [Residues 594−600 also participate in tetramer interactions but are ordered in one subunit within a dimer only (α_a) and are sandwiched between two crystallographically related tetramers; thus the ordering of these residues is likely a consequence of crystal packing.] Amino-terminal segments 2−10 and 26−32 bury 850 Å^2/monomer and pack against and form numerous hydrogen bonds with the αB1 helix of the α_d subunit (Figures 5 and 6). In addition, the αB3 helix of the α_d subunit interacts with the α_a subunit via three hydrogen bonds between K260 of the α_d subunit and K26, R29, and E31 of the α_a subunit (Figure 6). A small contribution (370 Å^2/monomer) is provided by residues 496−497 and 553−556 which interact with the corresponding residues of a symmetry-related monomer across the tetramer interface. Hydrogen bonds are formed between the side chains of H497 and Y555 and between the main chain carbonyl oxygen and side chain amide nitrogen groups of the N553 pairs. In contrast to

[4] Residues 2−593 only were used to calculate buried surfaces for *Ascaris* ME; residues 594−600 of the α_a monomer, which were not observed in the α_b monomer, were not included as the conformation of these residues is likely a consequence of crystal packing and may not reflect the actual conformation in solution.

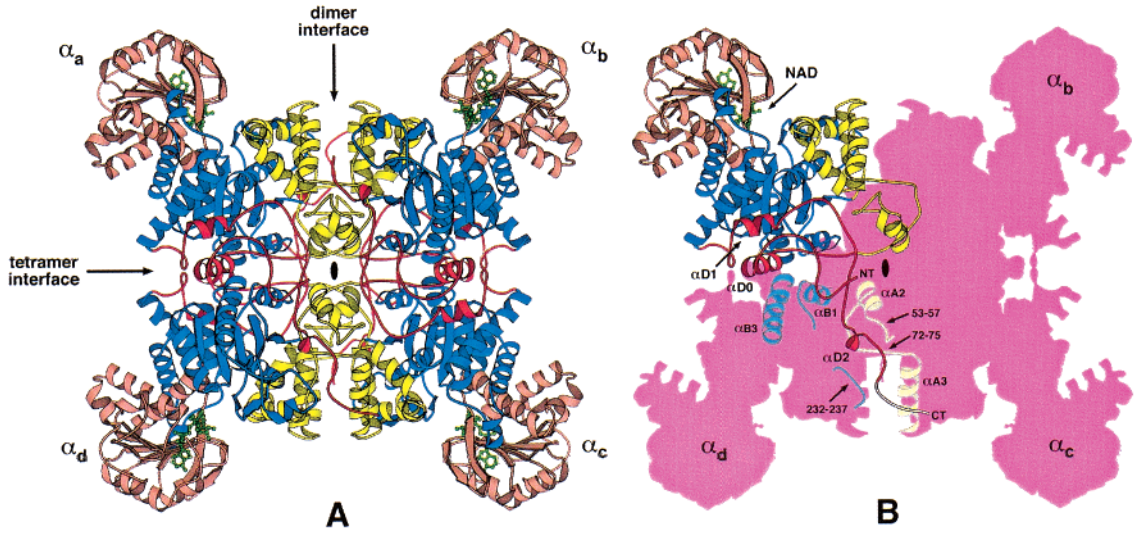

FIGURE 5: Structure of the tetramer of *Ascaris* m-NAD-ME in complex with NAD. (A) Ribbon diagram of the tetramer viewed down one 2-fold axis. The domains within each monomer are colored as per Figure 2, and the dimer and tetramer interfaces are indicated. The four subunits are labeled α_a, α_b, α_c, and α_d. The black oval indicates the position of the 2-fold axis corresponding to the axis *Y* in Figure 2. (B) The same view as in (A) except that three of the subunits (α_b, α_c, and α_d) are shown in silhouette only in order to indicate the locations of the N- and C-termini and the D domain of monomer α_a within the tetramer. Regions of subunit α_c and α_d that are involved in tetramer interactions with subunit α_a are also shown, shaded in lighter colors. C-Terminal residues that are present only in the α_a subunit (594−600) are colored white.

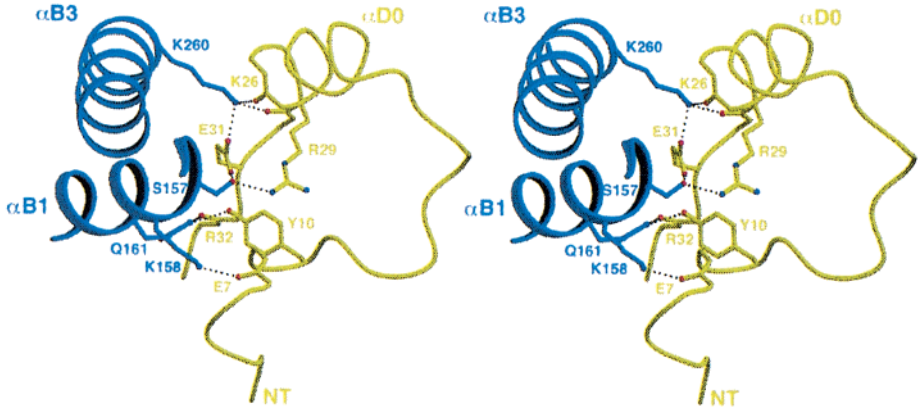

FIGURE 6: Tetramer interactions in *Ascaris* ME involving the amino-terminal residues of domain D. D domain residues (2−36) of the α_a subunit are colored yellow, and B domain residues of the α_d subunit are colored blue. Secondary structures and key amino acid residues are labeled. Hydrogen bonds are indicated by dashed lines. [This figure and Figure 7 were rendered using MOLSCRIPT (*49*) and RASTER3D (*50*).]

human ME, no exo NAD binding sites are present within the tetramer interface.

Comparison between the Ascaris and Human ME Binary Complexes. Ascaris and human MEs have similar sequences, architecture, and topology. A comparison between the structures of *Ascaris* and human ME binary complexes indicates that, with the exception of the D domain, their domain structures are similar, but the positions of their C domains relative to the A domain/B domain core differ. Omitting the D domain and segments that contain deletions (371−372, 387−388, 467−468) or an insertion (156−157) relative to human ME, the α carbons of the A, B, and C domains of *Ascaris* ME superimpose to the corresponding human ME residues with a root mean square (rms) difference of 1.05 Å. The individual domains superimpose to their human homologues with an rms difference of 0.75 Å (A domain), 0.92 Å (B domain), and 0.89 Å (C domain). Ignoring the D domains, the most extensive differences within each domain are found in the C domain segment 369−389 (which contains three deletions relative to human ME) and C domain loops 315−321 and 406−410. Superposition of the A and B domains together gives an rms difference of 0.92 Å relative to the corresponding human domains and indicates that the relative orientations of these two domains and those of the corresponding human ME domains are quite similar. In contrast, the respective C domains have different positions with respect to the A and B domains (Figure 7). The C domain of *Ascaris* ME is shifted such that the active site cleft formed between the C and B domains is widened up to 3.5 Å relative to human ME; this opening then leads to the differences in the NAD binding interactions discussed above, in particular, the absence of any interaction between R181 (human R165) and NAD. The more open nature of the *Ascaris* ME active site may be a consequence of differences in sequence, crystal packing or may be linked to differences in quaternary structure. Both of the crystallographically independent monomers of *Ascaris* ME have distinctly different crystallographic environments in the regions of their respective C domains but have similar structures; it is thus unlikely that crystal packing is respon-

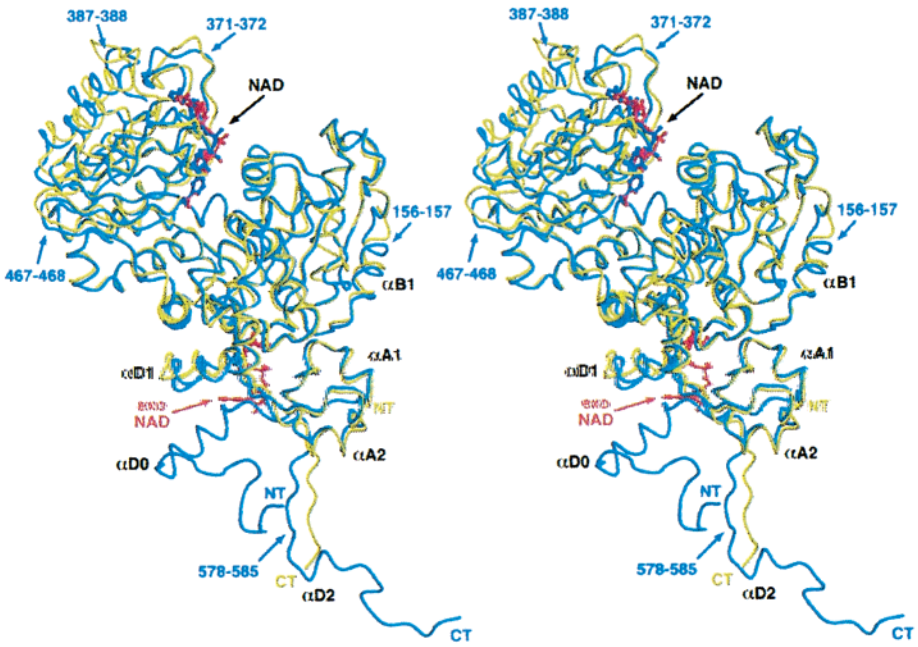

FIGURE 7: Superposition of the CA traces of the monomers of *Ascaris* (blue) and human (yellow) m-NAD-ME. The NAD bound to *Ascaris* ME is colored blue, and the NADs bound to human ME are colored red. The exo NAD from human ME is labeled. Segments containing deletions or insertions in *Ascaris* ME relative to human ME are indicated with blue labels. The location of the C-terminal segment containing *Ascaris* ME residues 578−585 is also indicated.

sible for the differences observed between the human and *Ascaris* active sites. The C domain has three small deletions (371-X-372, 387-X-X-388, 467-X-468) relative to the human enzyme (Figure 7). The deletions are located along the outer surface of the top of the C-domain, lie far from the active site, and are not involved in either domain or subunit interactions. In human ME, two residues (373−374) are inserted between the residues corresponding to residues 387 and 388 in *Ascaris* ME; the absence of these residues in *Ascaris* ME permits this region to pack more closely to the body of the C domain.

The most notable difference between the *Ascaris* and human MEs is in the D domain (Figure 7). In addition to the extra residues at the termini of the *Ascaris* D domain, the conformation of the residues homologous to those present in human ME differs. When the two enzymes are superimposed by their A and B domains, carboxyl-terminal segment 578−585 of *Ascaris* ME is shifted by up to 8.3 Å relative to the homologous human ME residues and has moved toward the αD1 helix (Figure 7). Likewise, the αD1 helix has moved slightly in the direction of the D domain carboxyl residues. Both of these changes can be attributed to new interactions made with the additional amino-terminal residues of the D domain.

The dimer interfaces in *Ascaris* and human ME are identical with the exception of small differences in one loop (*Ascaris*, 137−145; human, 123−131), and the amounts of buried surface area are similar (*Ascaris*, 1900 Å^2/monomer; human, 1800 Å^2/monomer). In contrast, the surface area buried on tetramer formation from dimers in *Ascaris* ME is increased by 170% relative to human ME (*Ascaris*, 3000 Å^2/monomer; human, 1100 Å^2/monomer). The regions of the tetramer interface that involve the homologous carboxyl-terminal segments of the D domains (*Ascaris*, 578−585; human, 566−573) are similar and bury similar surface areas (*Ascaris*, 1050 Å^2/monomer; human, 950 Å^2/monomer). The larger tetramer interface in *Ascaris* ME is due to the increased size of the D domain of *Ascaris* ME as a consequence of additional residues at the amino and carboxyl termini; these residues provide 1600 Å^2/monomer of additional buried surface within the tetramer interface. (Carboxyl terminal residues 574−584 of human ME may correspond to some of these residues but are disordered in the human ME structures.) The additional amino-terminal residues (2−32) provide 850 Å^2/monomer of new buried surface. In *Ascaris* ME helix αB1 contains an insertion (V156−S157) relative to human ME, which lengthens this helix (Figure 7) and provides new tetramer interactions with the amino-terminal residues of domain D. In particular, the side chain of S157 is hydrogen bonded to the side chains of D domain residues R29 and E31 (Figure 6), and the side chain of V156 fills a cavity within the interface.

Comparison of the tetramer organizations of the *Ascaris* and human ME binary complexes indicates that *Ascaris* ME is more flattened relative to human ME (Figure 8). This is a consequence of both the difference in the positions of the respective C domains relative to the A domain/B domain cores and a difference in the positions of the dimers within each tetramer. When the α carbons of the corresponding A and B domains of a single *Ascaris* ME dimer are superimposed on the corresponding human ME residues, the β sheet cores of each dimer are well aligned, indicating that the monomers that compose each dimer are positioned almost identically in both MEs. In contrast, the positioning of two dimers relative to each other differs between the two enzymes. After the superposition of single dimers described above is performed, a rotation of approximately 10° about the axis along the dimer interface is required in order to bring the second pair of dimers into superposition.

A key difference between the two enzymes is that the human enzyme is inhibited by ATP, while the *Ascaris* enzyme is not (*37*). The positions of the adenosine moiety

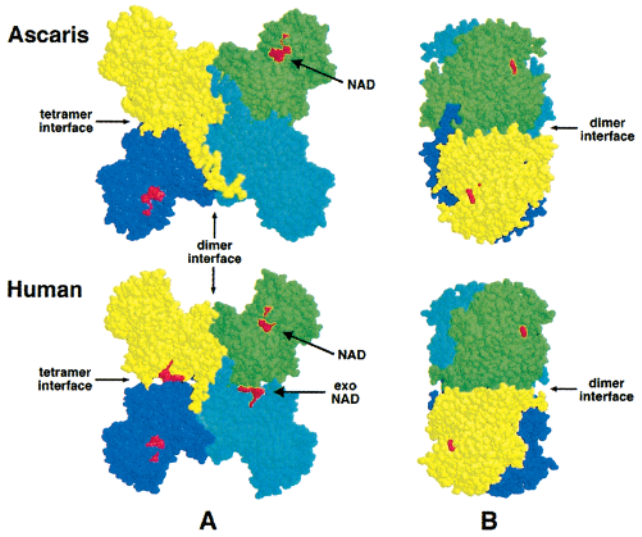

FIGURE 8: Space-filling models of *Ascaris* and human m-NAD-ME tetramers in complex with NAD. (A) *Ascaris* and human m-NAD-ME viewed down one noncrystallographic 2-fold axis (corresponding to axis *Y* in Figure 2) showing both the dimer and tetramer interfaces (this orientation is identical to that shown in Figure 5). The location of the NADs within the active sites and the exo NAD positions in human ME are indicated. (B) *Ascaris* and human m-NAD-ME viewed down the noncrystallographic 2-fold axis that lies in the plane of the dimer interface (corresponding to axis *Z* in Figure 2).

within the exo NAD binding sites in human ME (Figures 7 and 8A) are thought to correspond to the regulatory ATP binding sites. These sites are located within the tetramer interface. No NAD molecules are bound at the corresponding sites in *Ascaris* ME. Comparison of this region with the corresponding region in human ME indicates two reasons that there are no exo NAD sites in *Ascaris* ME. First, the αD0 helix in *Ascaris* ME blocks solvent access to the exo NAD site. Second, the side chain of W213 in *Ascaris* (human R187) fills the volume that is occupied by the adenine moiety of NAD in human ME and thus would prevent NAD binding. The absence of NAD binding within the tetramer interface of *Ascaris* ME may, in part, permit its altered quaternary structure relative to that of human ME.

DISCUSSION

The structure of mitochondrial NAD-ME from *A. suum* in binary complex with NAD will be discussed in concert with chemical and mutagenic studies and by comparison with structures of human mitochondrial NAD-ME−ligand complexes.

NAD is bound to *Ascaris* ME in a partially folded conformation that allows a close approach of the nicotinamide ring to the pyrophosphate moiety. Indeed, the distance between N1 of the nicotinamide ring and NO2 (Figure 3 and Table 2) of the phosphate α to the nicotinamide ribose is 5.7 Å [compared to a value of 5.2 Å in 6PGDH (*38*)], suggesting an electrostatic interaction between the two that could contribute to the overall binding energy and the final bound conformation. The bound conformation of NAD is reminiscent of the conformation of bound NADP in the E·NADP complex of 6-phosphogluconate dehydrogenase (*38*). Reduction of the nicotinamide ring will thus eliminate this electrostatic interaction, and this may have consequences to the overall mechanism of oxidative decarboxylation.

The localization of *Ascaris* (and other) m-NAD-ME to mitochondria implies that NAD is the cofactor used during catalysis in vivo. However, *Ascaris* m-NAD-ME can use either NAD or NADP in vitro (*14*). An acidic residue, D361, is located near the 2′-OH group of the adenosine moiety of NAD (Figure 3) and, based on work with other NAD or NADP binding proteins (*39*), might be expected to exclude the 2′-phosphate group of NADP from the active site and hence confer specificity for NAD. However, the side chain of D361 is pointed away from the 2′-OH position and makes a salt bridge with R370. Thus room is available for either NAD or NADP to bind. Aspartate 361 is conserved in all MEs regardless of their dinucleotide specificity and thus appears to play no role in dinucleotide specificity as was noted with respect to the homologous residue (D345) in human ME (*17*). However, in *Ascaris* m-NAD-ME, D361, when mutated to Ala, gives a greater than 20-fold increase in K_{NAD} with little, if any, change observed in V/E_t, K_{malate}, or K_{Mg} (*40*). This indicates that this residue affects NAD binding despite the absence of a direct interaction with NAD. A likely explanation for this effect is the loss of the salt bridge between D361 and R370 (which is also highly conserved in MEs). This interaction stabilizes one of the loops forming the adenosine binding site (361−362), and its loss would be expected to lower binding affinity for NAD without affecting catalytic interactions. Other residues may also affect binding specificity (or the lack thereof) in MEs. Kuo et al. (*41*) have pointed out that NADP-dependent ME isoforms all have a conserved lysine at a sequence position corresponding to H377 in *Ascaris* and Q362 in human m-NAD-MEs, whereas dual specificity MEs have heterogeneous residues at this position. This observation, combined with mutational and modeling studies using pigeon c-NADP-ME, led them to propose that, in NADP-dependent MEs, NADP specificity is conferred by lysine residues at this position. Mitochondrial NAD-MEs of *Ascaris* and other species may have no need to exhibit strict specificity for NAD due to the high concentration of NAD relative to NADP within mitochondria, and thus the residue at the corresponding position would not need to be constrained to be lysine.

NAD is bound to the active site of *Ascaris* ME with the *re* face of the cofactor directed toward solvent. Since hydride transfer is from C-2S of L-malate to the *re* face of the cofactor, the metal ion and malate must be bound in the space in front of NAD. In agreement with the proposed location, metal ion, oxalate, tartronate, and ketomalonate occupy this site in structures of the closed form of the human enzyme [Figure 3 (*20*)]. The approximate locations of the metal ion and malate binding sites in *Ascaris* ME can thus be approximately located by superposition with human ME and are indicated in Figure 4.

In the quaternary structure of the human enzyme, three acidic residues (E255, D256, and D279) are directly coordinated to Mn^{2+}, as well as to both carboxylate moieties of oxalate [Figure 4 (*20*)]. The corresponding residues in *Ascaris* ME (E271, D272, and D295) are completely conserved and likely have a similar metal binding role. However, mutation of two of these residues, D272 and D295, to Ala gives only marginal changes in K_{Mg}, and thus other residues may be able to compensate for the loss of interaction and or charge. In addition, it is not known whether the ligands

Scheme 2

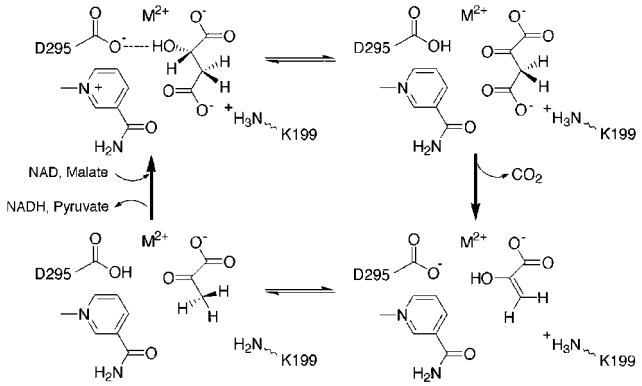

to the metal ion are the same at each of the three reaction steps. Interestingly, mutation of D178 (a potential second-sphere residue) to Ala exhibits a K_{Mg} about 50-fold greater than that of the wild-type enzyme, suggesting that charge and/or local structure of the active site is important for metal ion binding (*36*). In the quaternary complex of the human enzyme with oxalate, the oxalate binding residues (K183, R165, N421, and N467) are likely to perform similar roles in binding malate. All of these residues are conserved in *Ascaris* ME (K199, R181, N434, and N479) and, likewise, may have similar roles. In agreement with this proposal, in *Ascaris* ME, K_{malate} increases by about 10-fold when K199 is changed to Ala (*42*). In addition, K_{malate} increases by $\geq$500-fold when D295 is changed to Ala (*40*). These data were interpreted in terms of hydrogen-bonding interactions between D295 and the 2-hydroxyl of malate and between K199 and the β-carboxylate of malate. (During catalysis, the latter interaction between K199 and malate must be eliminated prior to decarboxylation.) The quaternary complex of the human enzyme with oxalate shows both carboxylates directly coordinated with Mn^{2+} [Figure 4 (*20*)], which implies that malate is bound to the enzyme such that its hydroxyl and α-carboxylate interact directly (or initially in a second-sphere coordination) with the metal ion. In *Ascaris* ME, spin−echo EPR experiments with Mn^{2+} as the divalent metal ion and L-malate specifically deuterated at C-2, C-3S, and C-3R indicate that the metal ion is in the vicinity of the C-2 hydroxyl of L-malate (*5*), which supports the hypothesis that malate also binds the metal ion in *Ascaris* ME.

A three-step mechanism for the reaction of ME has been proposed (*43*; Scheme 2) and is supported by substantial chemical and mutagenic studies (*42*−*47*). In the first step, malate is oxidized to oxaloacetate with concomitant reduction of NAD to NADH. The oxidation is facilitated by general base catalysis via an enzyme side chain that accepts a proton from the 2-hydroxyl of L-malate. This group functions to shuttle the proton between itself and the substrate oxygen, alternately acting as general base and general acid. The role of the metal ion in the oxidation step is not known with any certainty. In the second step, oxaloacetate is decarboxylated to enolpyruvate with a Lewis acid assist from Mg^{2+} and general acid protonation of C-2. In the final step, enolpyruvate is tautomerized to the ketone catalyzed by the general base and a second enzyme side chain acting as a general acid to protonate C-3. The mechanism requires enzyme residues positioned to serve as a catalytic base for the first step, and as a catalytic acid for the third step, as well as groups that will serve to bind and orient substrates for the subsequent catalytic steps.

Mutagenic studies have identified the side chains of D295 and K199 as the general base and general acid in the *Ascaris* enzyme. The general base, D295, when replaced with Ala, gave a 10^4-fold decrease in V/E_t and a 10^7-fold decrease in $V/K_{malate}E_t$, with little or no change in K_{Mg} (*40*). This residue may also interact with the metal ion at some point along the reaction pathway, as indicated by its role in binding Mn^{2+} in the quaternary complex of the human enzyme with oxalate. The general acid is K199; changing K199 to Ala gives a 10^5-fold decrease in V/E_t and a 10^6-fold decrease in $V/K_{malate}E_t$, while a change to Arg gives only a 10-fold decrease in V/E_t, which is expected since Arg can replace Lys as a general acid (*42*). As noted, in the quaternary complex of the human enzyme with oxalate, the side chain amino group of the homologous residue (K183) is hydrogen bonded to one of the oxalate carboxylate groups, and the authors have also proposed that this residue may act as the catalytic acid. As the *Ascaris* ME structure presented here represents the open form of the enzyme, the locations of K199 and D295 do not provide structural information regarding the roles of these residues during catalysis, and further structures will be required in order to definitively establish their roles.

Other residues may also be involved in catalysis. Tyrosine 126 (Y112 in the human enzyme) is in close proximity to K199 (Figure 4) and was thought to be a candidate for either the general base or acid, but recent mutagenesis studies have eliminated it as a candidate (*42*). The Y126F mutant gives a decrease in V/E_t by only a factor of 1000, and on the basis of partitioning of the oxalacetate intermediate, the ratio of pyruvate to malate produced from the E·NADH·Mg·OAA complex is not changed compared to that of the wild-type enzyme. This residue is conserved in all MEs and is the sole residue that is contributed to the active site by the A domain; its role thus remains a mystery.

The D domain of *Ascaris* ME is larger than that of human ME and increases the surface area involved in tetramer formation. Studies using pigeon liver ME have shown that MEs may undergo a monomer ↔ dimer ↔ tetramer equilibrium in solution (*48*). The larger tetramer interface in *Ascaris* ME would be expected to favor the tetrameric state of the enzyme, and we speculate that the additional amino- and carboxyl-terminal residues function to promote tetramer formation. However, no biochemical studies concerning the oligomerization state of *Ascaris* ME are available. In a search of available nucleic acid and protein sequence databases, only the hypothetical ME gene from *Caenorhabditis elegans* (gi 7509972) had significant protein sequence homology to the amino-terminal residues of the D domain of *Ascaris* ME (68% identity/83% homology for the segment corresponding to *Ascaris* ME D domain residues 18−36; 68% identity/84% homology for *Ascaris* ME residues 18−605). The homologous *Caenorhabditis* amino-terminal sequence corresponds to residues forming the αDO helix and downstream regions; thus, this feature of MEs may be unique to phylum Nematoda. Other than increasing the strength of the tetramer interface and further stabilizing the quaternary state of the molecule, it is not obvious why this amino-terminal feature is present in phylum Nematoda but not others.

Structural studies have shown that human ME exhibits different ligand-dependent conformational forms. Comparison of the binary complex containing NAD with quaternary complexes containing NAD and different metal ion/substrate analogue pairs (Mg^{2+}/tartronate, Mn^{2+}/oxalate, or Mg^{2+}/ketomalonate) defined two states for the active site: an open form corresponding to the binary complex and a closed form corresponding to the quaternary complexes. The active site in the open form does not appear to be arranged to carry out metal binding or catalysis whereas active site residues in the closed form appear to be positioned to carry out both functions. The binary and quaternary complexes also differ in quaternary structure, and it was initially hypothesized that these quaternary differences were linked to changes at the active site. However, a third conformational form was observed in the ternary complex with NAD and the inhibitor Lu^{2+} (*19*). In this case the complex exhibited a mixed open/closed conformation in which the active site is in an open form similar to that of the open binary complex whereas the tetramer organization and subunit interactions are similar to those observed in the closed quaternary complexes. This observation was interpreted to imply that the conformational changes involved in active site closure and those involved in rearrangement of the tetramer are independent. In all of these structures a second NAD was bound to each of four exo NAD sites located within the tetramer interface.

The *Ascaris* ME structure differs from all of those thus far described for human ME complexes in both its tertiary and quaternary structure and thus represents a forth observed ME conformational state. The active site most closely corresponds to that of the open form of human ME but, as noted, is actually more open in that the width of the active site is larger and the contacts with NAD are made exclusively with the C domain. In human ME the transition between the open and closed forms of the active site is achieved primarily via a rigid body rotation of the C domain toward the B domain. Modeling of a closed form of *Ascaris* ME using the closed form of human ME as a pattern indicates that a similar rotation of the C domain in *Ascaris* ME would close the active site. This, and the conservation of key active site residues between *Ascaris* and human ME, indicates that the closed form of the active site in *Ascaris* ME is likely to be similar to that of human. The quaternary structure of *Ascaris* ME also differs from each of the three types of human ME complexes thus far described. This difference is manifested by rigid body rotations of the two dimers about the 2-fold rotation axis along the dimer interface. Surprisingly, the relative orientation of the two dimers in the open *Ascaris* ME binary complex is most similar to that of the closed human quaternary complex. The ensemble of human ME structures implies that quaternary changes are associated with different ligand states of the enzyme, but the relationship between these changes and catalysis remains unclear (*19*). Given that human ME exhibits different quaternary structures depending on its ligation state, it is possible that *Ascaris* ME also exhibits different quaternary states on ligand binding. However, the more extensive tetramer interactions in *Ascaris* ME would be expected to stabilize the quaterary state observed in the binary *Ascaris* ME complex, and it is thus possible that changes in the quaternary structure of *Ascaris* ME are more restricted. Although the additional residues in *Ascaris* ME increase the tetramer interface and affect quaternary structure, it is not apparent from the binary complex whether they would have any effect on the enzyme's catalytic ability or the active site's transition from the open to the closed state. Structures of other *Ascaris* ME−ligand complexes are needed to address these questions.

Several factors can be identified that contribute to the difference in the quaternary structure between *Ascaris* and human MEs. The most apparent of these is the increased size of the D domain in *Ascaris* ME. The additional residues at the amino terminus of this domain result in new tetramer interactions which support the new quaternary structure. In addition, the interactions between these residues and the carboxyl-terminal residues of the D domain lead to a shift in position of the carboxyl tail of the D domain (Figure 7). As the interactions between this tail and other subunits are similar in both human and *Ascaris* ME, the shift of this tail in *Ascaris* ME necessitates a different quaternary arrangement relative to human ME. In addition, the tetramer interfaces in all of the human ME structures contain NAD molecules bound at four exo NAD sites, whereas these sites are absent in *Ascaris* ME. In human ME the exo sites presumably correspond to inhibitory ATP binding sites. This implies that even the closed form human ME complexes may not correspond to the fully active state of the enzyme. Further crystallographic structures of *Ascaris* ME−ligand complexes may thus provide a picture of ME in the fully active state.

ACKNOWLEDGMENT

We thank the staff at the Cornell High Energy Synchrotron Source (CHESS) for assistance with data collection.

REFERENCES

1. Kulkarni, G., Cook, P. F., and Harris, B. G. (1993) *Arch. Biochem. Biophys. 300*, 231−237.
2. Rao, J. G. S., Coleman, D. E., Kulkarni, G., Goldsmith, E. J., Cook, P. F., and Harris, B. G. (2000) *Protein Pept. Lett. 7*, 297−304.
3. Hsu, R. Y. (1982) *Mol. Cell. Biochem. 43*, 3−26.
4. Moreadith, R. W., and Lehninger, A. L. (1984) *J. Biol. Chem. 259*, 6222−6227.
5. Tipton, P. A., Quinn, T. P., Peisach, J., and Cook, P. F. (1996) *Protein Sci. 5*, 1648−1654.
6. Drincovich, M. F., Casati, P., and Andreo, C. S. (2001) *FEBS Lett. 490*, 1−6.
7. Loeber, G., Infante, A. A., Maurer-Fogy, I., Krystek, E., and Dworkin, M. B. (1991) *J. Biol. Chem. 266*, 3016−3021.
8. Urbauer, J. L., Bradshaw, D. E., and Cleland, W. W. (1998) *Biochemistry 37*, 18026−18031.
9. Saz, H. J. (1981) *Annu. Rev. Physiol. 43*, 323−341.
10. Swierczynski, J., Stankiewicz, A., Scislowski, P., and Aleksandrowicz, Z. (1980) *Biochim. Biophys. Acta 612*, 1−10.
11. Voegele, R. T., Mitsch, M. J., and Finan, T. M. (1999) *Biochim. Biophys. Acta 1432*, 275−285.
12. Long, J. J., Wang, J. L., and Berry, J. O. (1994) *J. Biol. Chem. 269*, 2827−2833.
13. Sauer, L. A. (1973) *Biochem. Biophys. Res. Commun. 50*, 524−531.
14. Weiss, P. M., Gavva, S. R., Harris, B. G., Urbauer, J. L., Cleland, W. W., and Cook, P. F. (1991) *Biochemistry 30*, 5755−5763.
15. Karsten, W., and Cook, P. F. (2000) *Protein Pept. Lett. 7*, 281−286.
16. Xu, Y., Bhargava, G., Wu, H., Loeber, G., and Tong, L. (1999) *Structure 7*, 877−889.
17. Yang, Z., and Tong, L. (2000) *Protein Pept. Lett. 7*, 287−296.

18. Bhargava, G., Mui, S., Pav, S., Wu, H., Loeber, G., and Tong, L. (1999) *J. Struct. Biol. 127*, 72−75.
19. Yang, Z., Batra, R., Floyd, D. L., Hung, H. C., Chan, G. G., and Tong, L. (2000) *Biochem. Biophys. Res. Commun. 274*, 440−444.
20. Yang, Z., Floyd, D. L., Loeber, G., and Tong, L. (2000) *Nat. Struct. Biol. 7*, 251−257.
21. Saz, H. J. (1970) *J. Parasitol. 56*, 634−642.
22. Clancy, L. L., Rao, G. S. J., Finzel, B. C., Muchmore, S. W., Holland, D. R., Watenpaugh, K. D., Krishnamurthy, H. M., Sweet, R. M., Cook, P. F., Harris, B. G., and Einspahr, H. M. (1992) *J. Mol. Biol. 226*, 565−569.
23. Karsten, W. E., and Cook, P. F. (1994) *Biochemistry 33*, 2096−2103.
24. Otwinowski, Z., and Minor, W. (1997) *Methods Enzymol. 276*, 307−326.
25. Rossmann, M. G. (1972) *The Molecular Replacement Method: A collection of papers on the use of noncrystallographic symmetry*, Gordon and Breach, New York.
26. Collaborative Computational Project, Number 4 (1994) *Acta Crystallogr. D50*, 760−763.
27. Brünger, A. T., Adams, P. D., Clore, G. M., Gros, P., Grosse-Kunstleve, R. W., Jiang, J.-S., Kuszewski, J., Nilges, M., Pannu, N. S., Read, R. J., Rice, L. M., Simonson, T., and Warren, G. L. (1998) *Acta Crystallogr. D54*, 905−921.
28. Read, R. J. (1986) *Acta Crystallogr. A42*, 140−149.
29. Jones, T. A., Zou, J. Y., Cowan, S. W., and Kjeldgaard, M. (1991) *Acta Crystallogr. A47*, 110−119.
30. Jiang, J. S., and Brünger, A. T. (1994) *J. Mol. Biol. 243*, 100−115.
31. Brünger, A. T. (1992) *Nature 355*, 472−475.
32. Laskowski, R. A., MacArthur, M. W., Moss, D. S., and Thornton, J. M. (1993) *J. Appl. Crystallogr. 26*, 283−291.
33. Rossmann, M. G., Moras, D., and Olsen, K. W. (1974) *Nature 250*, 194−199.
34. Rao, J. G. S., Harris, B. G., and Cook, P. F. (1985) *Arch. Biochem. Biophys. 241*, 67−74.
35. Rao, J. G. S., Kong, C. T., Benjamin, R. C., Harris, B. G., and Cook, P. F. (1987) *Arch. Biochem. Biophys. 255*, 8−13.
36. Karsten, W. E., Chooback, L., Liu, D., Hwang, C.-C., Lynch, C., and Cook, P. F. (1999) *Biochemistry 38*, 10527−10532.
37. Landsperger, W. J., and Harris, B. G. (1976) *J. Biol. Chem. 251*, 3599−3602.
38. Adams, M. J., Ellis, G. H., Gover, S., Naylor, C. P., and Phillips, C. (1994) *Structure*, 651−668.
39. Scrutton, N. S., Berry, A., and Perham, R. N. (1990) *Nature 343*, 38−43.
40. Karsten, W. E., Hwang, C.-C., and Cook, P. F. (1999) *Biochemistry 38*, 4398−4402.
41. Kuo, C. C., Tsai, L. C., Chin, T. Y., Chang, G. G., and Chou, W. Y. (2000) *Biochem. Biophys. Res. Commun. 270*, 821−825.
42. Liu, D., Karsten, W. E., and Cook, P. F. (2000) *Biochemistry 39*, 11955−11960.
43. Kiick, D. M., Harris, B. G., and Cook, P. F. (1986) *Biochemistry 25*, 227−236.
44. Park, S. H., Kiick, D. M., Harris, B. G., and Cook, P. F. (1984) *Biochemistry 23*, 5446−5453.
45. Park, S.-H., Harris, B. G., and Cook, P. F. (1986) *Biochemistry 25*, 3752−3759.
46. Chen, C.-Y., Harris, B. G., and Cook, P. F. (1988) *Biochemistry 27*, 212−219.
47. Mallick, S., Harris, B. G., and Cook, P. F. (1991) *J. Biol. Chem. 266*, 2732−2738.
48. Chang, G.-G., Huang, T.-M., and Chang, T.-C. (1988) *Biochem. J. 254*, 123−130.
49. Kraulis, P. J. (1991) *J. Appl. Crystallogr. 24*, 946−950.
50. Merritt, E. A., and Murphy, M. E. P. (1994) *Acta Crystallogr. D50*, 869−873.

BI0255120